# Kinetics and Mechanism of Redox-Coupled, Long-Range Proton Transfer in an Iron−Sulfur Protein. Investigation by Fast-Scan Protein-Film Voltammetry

**Judy Hirst,[†] Jillian L. C. Duff,[†] Guy N. L. Jameson,[†] Mary A. Kemper,[‡] Barbara K. Burgess,[‡] and Fraser A. Armstrong*,[†]**

*Contribution from the Department of Chemistry, Inorganic Chemistry Laboratory, Oxford University, South Parks Road, Oxford, OX1 3QR, England, and the Department of Molecular Biology and Biochemistry, University of California, Irvine, California 92717-3900*

*Received February 3, 1998*

**Abstract:** Fast-scan protein-film voltammetry has been used to study and deconvolute the kinetics of proton-coupled electron transfer to and from the [3Fe−4S] cluster in *Azotobacter vinelandii* Ferredoxin I (*Av* Fd I). This crystallographically defined 7Fe ferredoxin contains a [3Fe−4S] cluster which takes up a proton when in its reduced (0) state. Results conform to a model for stepwise electron and proton transfers. Electron transfer to the cluster drives its protonation, whereas the rate of reoxidation of $[3Fe-4S]^0$-$H^+$ is controlled by the rate of release of the proton. The cluster is buried and inaccessible to solvent water molecules; an aspartate (D15) is located on the protein surface but otherwise proton transfer occurs across an aprotic barrier. The D15N mutant, in which this aspartate is replaced by asparagine, has also been studied. Rate constants for proton transfer in each direction and the accompanying energetics (reduction potentials and interdependent p*K* values of the cluster and aspartate) have been determined simultaneously by modeling voltammetric peak positions (measured over a range of scan rate and pH) using numerical (digital) simulation. For comparison, rates of proton-gated oxidation were measured independently using stopped-flow spectrophotometry. Proton transfer between the cluster and bulk water occurs over 100 times faster in the native protein than in D15N, and the kinetics are described by a mechanism in which the proton is transferred using the aspartate carboxylate. Lack of an H/D isotope effect suggests that this group acts as a short-range courier. The system provides an intriguing functional model for redox-driven proton pumps, being both well-defined at the molecular level and amenable to detailed study by film voltammetry.

## Introduction

Coupled electron−proton transfer reactions are central to enzymatic redox catalysis and have a special place in bioenergetics where respiratory electron-transport chains generate a transmembrane proton gradient.[1,2] An understanding of how this coupling is produced and organized by the protein may be stated in terms of (a) measurement and deconvolution of the complex interlinked kinetics and energetics and (b) defining, at the detailed structural level, the mechanisms not only of coupling but also of long-range proton transfer. The overall thermodynamics of proton-coupled reactions are relatively straightforward, being revealed via the familiar pH dependence of reduction potentials.[3] On the other hand, the kinetics of redox-coupled reactions may be very convoluted[4,5] and determinations of energetics and rates of reaction of transient intermediate species present many experimental challenges. The primary coupling process may involve protonation of the redox center (as in quinones), of metal-site ligands, or of residues remote from the site of electronation. Proton transfer itself may occur in concert with electron transfer or may be rate-determining and "gate" electron transfer since, unlike electrons, the tunneling distance of protons is small[6] and the protein offers resistance in all but special cases. Proton transport within a protein generally involves conduction along a "wire" created by a hydrogen-bonded channel comprising protein bases and/or water molecules.[7,8] Alternatively, protons can be "shuttled" across an insulating barrier by bases that are mobile within the protein (the "piggyback" mechanism).[9] Energized changes in conformation can be used to "gate" proton transfer and produce a pump.[9−11]

[†] Oxford University.

[‡] University of California.

(1) Mitchell, P. *Nature* **1961**, *191*, 144−148: Williams, R. J. P. *Biochim. Biophys. Acta* **1991**, *1058*, 71−74.

(2) Babcock, G. T.; Wikström, M. *Nature* **1992**, *356*, 301−309. Malmström, B. G. *Acc. Chem. Res.* **1993**, *26*, 332−338: Ramirez, B. E.; Malmström, B. G.; Winkler, J. R.; Gray, H. B. *Proc. Natl. Acad. Sci. U.S.A.* **1995**, *92*, 11949−11951. Rich, P. R.; Meunier, B.; Mitchell, R.; Moody, A. J. *Biochim. Biophys. Acta* **1996**, *1275*, 91−95.

(3) Clark, W. M. *Oxidation Reduction Potentials of Organic Systems*; Williams and Wilkins: Baltimore, 1960.

(4) Verkhovsky, M. I.; Morgan, J. E.; Wikström, M. *Biochemistry* **1995**, *34*, 7483−7491. Brzezinski, P. *Biochemistry* **1996**, *35*, 5611−5615: Ädelroth, P.; Sigurdson, H.; Hallén, S.; Brzezinski, P. *Proc. Natl. Acad. Sci. U.S.A.* **1996**, *93*, 12292−12297.

(5) Graige, M. S.; Paddock, M. L.; Bruce, J. M.; Feher, G.; Okamura, M. Y. *J. Am. Chem. Soc.* **1996**, *118*, 9005−9016.

(6) Sarai, A.; DeVault, D. *Methods Enzymol.* **1986**, *127*, 79−91. Bahnson, B. J.; Klinman, J. P. *Methods Enzymol.* **1995**, *249*, 373−397.

(7) Nagle, J. F.; Morowitz, H. J. *Proc. Natl. Acad. Sci. U.S.A.* **1978**, *75*, 298−302: Nagle, J. F.; Tristam-Nagle, S. *J. Membr. Biol.* **1983**, *74*, 1−14. Schulten, Z.; Schulten, K. *Methods Enzymol.* **1986**, *127*, 419−438.

(8) Baciou, L.; Michel, H. *Biochemistry* **1995**, *34*, 7967−7972.

(9) Williams, R. J. P. *Annu. Rev. Biophys. Biophys. Chem.* **1988**, *17*, 71−97.

(10) Warshel, A. *Methods Enzymol.* **1986**, *127*, 578−587.

(11) Lanyi, J. K. *Nature* **1995**, *375*, 461−463.

S0002-7863(98)00380-1 CCC: $15.00 
Published on Web 07/03/1998

Redox-coupled proton transfer has been studied extensively in several complex enzymes for which the structure has been determined in one oxidation state. One example is cytochrome *c* oxidase, in which pathways conducting both scalar and vectorial protons have been identified from the structure and results of site-directed mutagenesis, for example, the replacement of Asp/Glu by Asn/Gln results in proton transfer being retarded.[12] The mechanism of the proton pump remains a question of great interest,[2,4] with hypotheses including the "histidine cycle" in which redox cycling of active-site $Cu_B$ induces protonation, dissociation, and reorientation of a relatively mobile imidazole ligand.[13,14] Another example is the photosynthetic reaction center of the purple bacterium *Rhodobacter sphaeroides*, in which transfer of electrons to a buried quinone is coupled to the transfer of protons from solvent.[15] Kinetic studies in conjunction with site-directed mutagenesis and quinone substitutions lead to a picture favoring stepwise electron and proton transfers, with the latter using conducting pathways provided by protein residue carboxylate groups and water molecules.[5,15−17] Other enzymes include nitrogenase, in which protons are involved in the reduction of dinitrogen to ammonia at a Mo−Fe−S cluster.[18] In addition to these complex systems, insight into the coupling problem at a localized level is being sought with the use of synthetic nonprotein models.[19]

Protein-film voltammetry affords the means to measure, deconvolute, and quantify the kinetics and thermodynamics of coupled electron-transfer reactions from a single set of experiments.[20,21] The pattern of reactions and gating is recognizable from the forms of the oxidative and reductive current responses, obtained as the potential is cycled at rates up to and exceeding 100 V $s^{-1}$.[21] Suitable systems with which to investigate the proton-coupling problem in this way have the following attributes: they display proton-coupled electron transfer to a buried redox center, they are structurally defined in the relevant oxidation states, they are amenable to systemmatic alteration by genetic engineering, and naturally, they exhibit fast interfacial electron transfer at an electrode. As will be described, such a system is provided by the small 7Fe ferredoxin from *Azotobacter vinelandii*.

Although iron−sulfur (Fe−S) clusters are well-established agents of electron transfer[22] and are implicated in proton-transfer catalysis, as in nitrogenase,[18ab] their ability to bind or transfer protons in certain cases is only recently coming to light.[23−32] An interesting example is provided by [3Fe−4S] centers, which display extensive proton-coupled electron-transfer activity.[24−32] The oxidized (all Fe(III)) $[3Fe-4S]^{+}$ level takes up one electron to give the normal reduced form, $[3Fe-4S]^{0}$, or three electrons to give a novel state, $[3Fe-4S]^{2-}$, which formally contains three Fe(II).[24] As further quantified by the pH dependence of reduction potentials, one and three protons are taken up, respectively.[24] This paper is concerned with the one-electron reduced $[3Fe-4S]^{0}$ cluster, for which the uptake of a single proton has been quantified by voltammetry and studied independently by MCD.[25−31] In this context, the 7Fe ferredoxin (Fd I) from *A. vinelandii* (*Av*), which contains one [3Fe−4S] and one [4Fe−4S] cluster, has been investigated in the greatest detail. Although the exact site of protonation has not so far been established,[32] it is certain from the magnitude of MCD spectral changes,[27−31] the absence of structural changes (as determined by X-ray crystallography on the 1+ and 0 oxidation levels at different pH values[33,34]), and studies with mutants lacking nearby ionizable residues[26] that the proton is bound within the molecular framework of the core or the cysteine ligands. In native *Av* Fd I, the p*K* for this process is 7.8,[26] necessitating that, below this value, electron transfer to the cluster is accompanied by spontaneous proton transfer. However, the [3Fe−4S] cluster is buried ca. 8 Å below the protein surface and is not accessible to solvent water molecules.[33,34] As shown in Figure 1, the nearest ionizable residue is aspartate-15 (D15) which is salt-bridged to a lysine residue (K84) at the surface. From NMR titrations (8 °C) the p*K* of the D15 carboxylate is reported to be 5.4 for the oxidized protein.[35] The structure of the reduced $[3Fe-4S]^{0}$ form at pH 6.3 shows that one oxygen atom of D15 (O2) is located 4.85 Å from one of

(12) Fetter, J. R.; Qian, J.; Shapleigh, J.; Thomas, J. W.; García-Horsman, A.; Schmidt, E.; Hosler, J.; Babcock, G. T.; Gennis, R. B.; Ferguson-Miller, S. *Proc. Natl. Acad. Sci. U.S.A.* **1995**, *92*, 1604−1608.

(13) Iwata, S.; Ostermeier, C.; Ludwig, B.; Michel, H. *Nature* **1995**, *376*, 660−669. Ostermeier, C.; Iwata, S.; Michel, H. *Curr. Opin. Struct. Biol.* **1996**, *6*, 460−466.

(14) Morgan, J. E.; Verkhovsky, M. I.; Wikström, M. *J. Bioenerg. Biomembr.* **1994**, *26*, 599−608.

(15) Okamura, M. Y.; Feher, G. *Annu. Rev. Biochem.* **1992**, *61*, 861−896.

(16) Okamura, M. Y.; Feher, G. *Proc. Natl. Acad. Sci. U.S.A.* **1986**, *83*, 8152−8156. Paddock, M. L.; Rongey, S. H.; McPherson, P. H.; Juth, A.; Feher, G.; Okamura, M. Y. *Biochemistry* **1994**, *33*, 734−745. McPherson, P. H.; Schönfeld, M.; Paddock, M. L.; Okamura, M. Y.; Feher, G. *Biochemistry* **1994**, *33*, 1181−1193.

(17) Takahashi, E.; Wraight, C. A. *Proc. Natl. Acad. Sci. U.S.A.* **1996**, *93*, 2640−2645. Takahashi, E.; Wraight, C. A. *Biochemistry* **1992**, *31*, 855−866. Takahashi, E.; Wraight, C. A. *Biochim. Biophys. Acta* **1990**, *1020*, 107−111.

(18) (a) Burgess, B. K.; Lowe, D. J. *Chem. Rev.* **1996**, *96*, 2983−3011. (b) Peters, J. W.; Stowell, M. H. B.; Soltis, S. M.; Finnegan, M. G.; Johnson, M. K.; Rees, D. G. *Biochemistry* **1997**, *36*, 1181−1187. See also: Rohlfs, R. J.; Huang, L.; Hille, R. *J. Biol. Chem.* **1995**, *270*, 22196−22207, for a recent example of a study of proton-gated electron transfer in an Fe−S flavoenzyme.

(19) Cukier, R. I. *J. Phys. Chem.* **1994**, *98*, 2377−2381; **1995**, *99*, 16101−16115; **1996**, *100*, 15428−15433. Kirby, J. P.; Roberts, J. A.; Nocera, D. G. *J. Am. Chem. Soc.* **1996**, *119*, 9230−9236.

(20) Armstrong, F. A.; Heering, H. A.; Hirst, J. *Chem. Soc. Rev.* **1997**, *26*, 169−179.

(21) Hirst, J.; Armstrong, F. A. Submitted for publication.

(22) Cammack, R. *Adv. Inorg. Chem.* **1992**, *38*, 281−322. Johnson, M. K. *Encyclopedia of Inorganic Chemistry*; King, R. B., Ed.; Wiley: Chichester, 1994; pp 1896−1915. Beinert, H.; Holm, R. H.; Münck, E. *Science* **1997**, *277*, 653−659.

(23) The Rieske center is an example of an Fe−S cluster in which electron transfer is linked to ligand (imidazole)-based proton transfer. See: Link, T. A.; Hagen, W. R.; Pierik, A. J.; von Jagow, G. *Eur. J. Biochem.* **1992**, *208*, 685−691.

(24) Duff, J. L. C.; Breton, J. L. J.; Butt, J. N.; Armstrong, F. A.; Thomson, A. J. *J. Am. Chem. Soc.* **1996**, *118*, 8593−8603.

(25) Butt, J. N.; Sucheta, A.; Martin, L. L.; Shen, B.; Burgess, B. K.; Armstrong, F. A. *J. Am. Chem. Soc.* **1993**, *115*, 12587−12588.

(26) Shen, B.; Martin, L. L.; Butt, J. N.; Armstrong, F. A.; Stout, C. D.; Jensen, G. M.; Stephens, P. J.; La Mar, G. N.; Gorst, C. M.; Burgess, B. K. *J. Biol. Chem.* **1993**, *268*, 25928−25939.

(27) (a) Breton, J. L.; Duff, J. L. C.; Butt, J. N.; Armstrong, F. A.; George, S. J.; Pétillot, Y.; Forest, E.; Schäfer, G.; Thomson, A. J. *Eur. J. Biochem.* **1995**, *233*, 937−946: (b) Fawcett, S. E. J.; Davis, D. E.; Breton, J. L. J.; Thomson, A. J.; Armstrong, F. A. submitted for publication.

(28) George, S. J.; Richards, A. J. M.; Thomson, A. J.; Yates, M. G. *Biochem. J.* **1984**, *224*, 247−251. Armstrong, F. A.; George, S. J.; Thomson, A. J.; Yates, M. G. *FEBS Lett.* **1988**, *234*, 107−110.

(29) Johnson, M. K.; Bennett, D. E.; Fee, J. A.; Sweeney, W. V. *Biochim. Biophys. Acta* **1987**, *911*, 81−94.

(30) Stephens, P. J.; Jensen, G. M.; Devlin, F.; Morgan, T. V.; Stout, C. D.; Burgess, B. K. *Biochemistry* **1991**, *30*, 3200−3209.

(31) Iismaa, S. E.; Vázquez, A. E.; Jensen, G. M.; Stephens, P. J.; Butt, J. N.; Armstrong, F. A.; Burgess, B. K. *J. Biol. Chem.* **1991**, *266*, 21563-21571.

(32) Hu, Z. G.; Jollie, D.; Burgess, B. K.; Stephens, P. J.; Münck, E. *Biochemistry* **1994**, *33*, 14475−14485.

(33) Stout, C. D. *J. Biol. Chem.* **1988**, *263*, 9256−9260; *J. Mol. Biol.* **1989**, *205*, 545−555.

(34) Stout, C. D. *J. Biol. Chem.* **1993**, *268*, 25920−25927.

(35) Cheng, H.; Grohmann, K.; Sweeney, W. V. *J. Biol. Chem.* **1990**, *265*, 12388−12392.

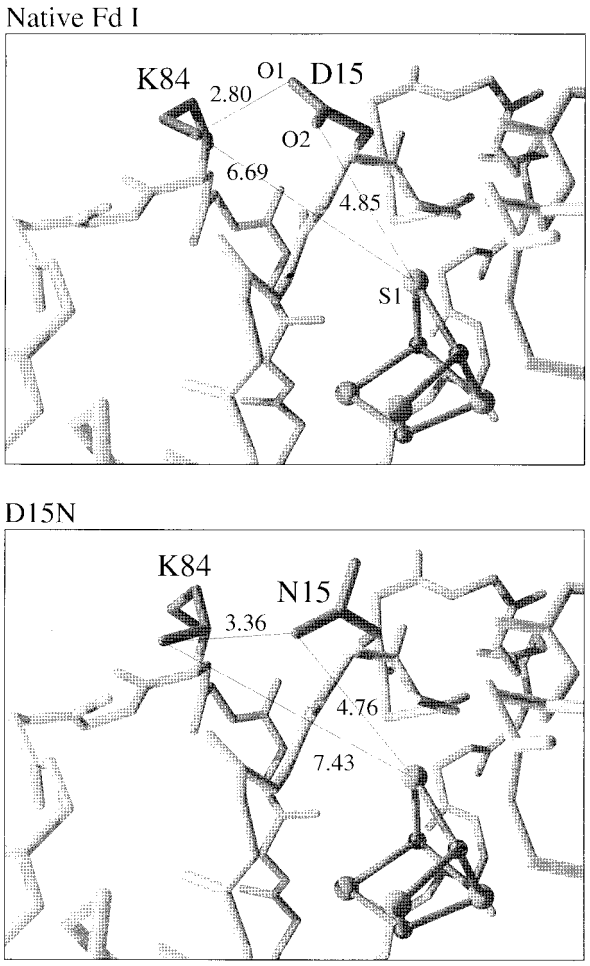


**Figure 1.** The "proton-transferring modules" of native *Av* Fd I (reduced form, pH 6) and D15N (oxidized form) showing the relative positions of surface residues D15 (or N15), K84, and the buried [3Fe−4S] cluster. See refs 26 and 34. The two structures are virtually superimposable except in the specific region of mutation. In native *Av* Fd I, there is a salt bridge between the D15 carboxylate (O1) and the side chain $NH_3^+$ of K84. In D15N this salt bridge is lost and the K84 ζ N atom forms a new hydrogen bond to the carbonyl of K85. Also shown are various interatomic distances (in angstroms): between the nearest $\mu_2$ sulfur (S1) on the cluster and D15 (O2); between K84 (ζ N) and D15 (O1) or N15; between K84 (ζ N) and S1. In D15N the ζ N atom of K84 moves into a position to form a hydrogen bond with the carbonyl group of K85.

the $\mu_2$ S atoms (S1) of the protonated [3Fe−4S]$^0$ cluster, and no other polar groups are found in the intervening region.[34] A similar structure is found for the oxidized form of the protein; by contrast, for the reduced form at pH 8.3 (in which the [3Fe−4S]$^0$ cluster is not protonated) O2 is moved away to 5.23 Å from the S atom.[34] The difference in electrostatics between addition of an electron alone and electroneutral reduction by an electron and accompanying proton is thus reflected in a structural response and suggests that there is some mobility in this region of the protein. Shown also in Figure 1 is the organization of residues in a mutant, D15N, in which aspartate-15 has been replaced by asparagine.[26] In this variant, the cluster p*K* is decreased to 6.9, the lower proton affinity reflecting the less favorable electrostatics expected after removing the nearby negative charge (the carboxylate group). As the following account will show, the two proteins represent, respectively, efficient and inefficient "modules" for long-range proton transfer within an anhydrous protein interior.

**Scheme 1.** Coupled Electron−Proton Transfer at a [3Fe−4S] Cluster

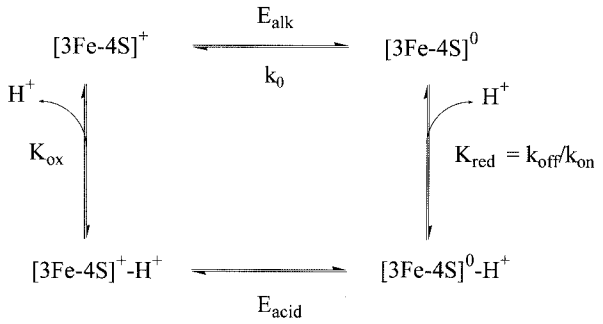


Scheme 1 depicts a generalized square scheme[36,37] which describes the coupled proton−electron transfer reactions occurring in *Av* Fd I. The system is defined (a) thermodynamically, by two reduction potentials for electron transfer (horizontal processes) and two equilibrium constants for proton transfer (vertical processes) and (b) kinetically, by the associated rate constants ($k_0$ for interfacial electron exchange and $k_{on}$ and $k_{off}$ for proton transfer at [3Fe−4S]$^0$ will be shown to be relevant).

In an earlier report we described preliminary experiments carried out on the D15N mutant, which showed that oxidation of the protonated reduced cluster [3Fe−4S]$^0$-H$^+$ is severely retarded in D15N relative to that of the native protein.[25,26] The voltammetry conformed to a stepwise mechanism in which electron transfer is controlled by the rate of deprotonation. Cluster protonation kinetics were linearly proportional to [H$^+$] while $k_{off}$ (3 s$^{-1}$) was pH-independent. In this earlier study, scan rates were limited to <1 V s$^{-1}$, at which speeds the voltammetry of the native *Av* Fd I appeared uncomplicated and reversible. The results demonstrated that efficient proton transfer requires aspartate-15 and suggested a crucial role for the carboxylate. In this paper, we report experiments on both native *Av* Fd I and the D15N mutant, using protein-film cyclic voltammetry carried out at scan rates up to 100 V s$^{-1}$.[21] The conclusions are supported by results obtained independently by stopped-flow spectrophotometry. A detailed description of the energetics and kinetics of the redox-coupled proton transfer is obtained, which provides insight into the operation of a proton shuttle and is relevant to the mechanism of redox-driven proton pumps.

## Experimental Section

Samples of native *Av* Fd I and the D15N mutant were obtained as described previously,[26] and purity was ensured by fast protein liquid chromatography (Pharmacia, FPLC) prior to experiments. For all studies, a common, 20 mM mixed buffer system (5 mM in each of MES, HEPES, TAPS, and acetate buffers) was used to achieve continuity throughout the entire pH range studied. Protein solutions for preparing films on electrodes contained (typically) 100 μM protein, 20 mM mixed buffer and 0.1 M NaCl, at pH 7.0, with polymyxin B sulfate (200 μg mL$^{-1}$) included as a coadsorbate to promote and stabilize the response obtained.[9] Cell solutions contained 20 mM mixed buffer with 0.1 M NaCl as supporting electrolyte and polymyxin B sulfate (200 μg mL$^{-1}$) to maintain equilibrium with the film. The pH of the cell solution was adjusted at 0 °C using dilute HCl or NaOH as necessary and rechecked after experimentation. Prior to voltammetry, the pyrolytic graphite edge (PGE) working electrode surface was

(36) Bond, A. M.; Oldham, K. B. *J. Phys. Chem.* **1983**, *87*, 2492−2502: Evans, D. H.; O'Connell, K. M. *Electroanal. Chem.* **1986**, *14*, 113−207.

(37) Hoffman, B. M.; Ratner, M. R. *J. Am. Chem. Soc.* **1987**, *109*, 6237−6243. Brunschwig, B. S.; Sutin, N. *J. Am. Chem. Soc.* **1989**, *111*, 7454−7465.

polished with 1 $\mu$m alumina, sonicated thoroughly, and washed with Millipore water (resistivity 18 MΩ·cm), and then a film of the protein was applied using a Pasteur pipet drawn to a fine capillary tip.[39]

The electrochemical cell was of all-glass construction and designed so that the Luggin capillary tip of the side arm housing the standard calomel reference electrode (SCE) could be reproducibly positioned normal to the working electrode surface at a distance of ca. 1 mm. The side-arm temperature was checked for each set of experiments, and we corrected potentials to the SHE scale using a standard formula.[38] The cell was enclosed in a Faraday cage to minimize electrical noise, thermostated at 0 °C using a water jacket, and purged with high-purity Ar. Remaining electrical noise was removed by Fourier transformation, provided that the electrochemical response and the noise were on sufficiently separate time scales. Control experiments, in which the data were also "smoothed" by averaging a large number of identical scans, showed that this procedure did not affect peak position or shape.

Analogue cyclic voltammetry was recorded using an Autolab electrochemical analyzer (Eco-chemie, Utrecht, The Netherlands) equipped with a PGSTAT 20 and fast analogue scan generator, in combination with a fast AD converter (ADC750). Effects of uncompensated cell resistance were minimized by decreasing the area of the working electrode to ca. 0.25 $mm^2$ [21] to reduce current magnitudes and by using the positive-feedback *iR* compensation function of the potentiostat, set at a value slightly below that at which current oscillations emerge.[40] Background (electrode) currents were subtracted using an in-house analysis program (H. A. Heering) which fits a cubic spline function[41] to the baseline in regions sufficiently far from the peak and assumes continuation of a similar, smooth function throughout the peak region.

Numerical modeling was carried out using a finite difference procedure.[21,42] Small steps in potential were simulated, and changes in the populations of the oxidized and reduced, protonated and deprotonated forms of the cluster were calculated. The simulation was assumed to have converged to the analogue limit when decreasing the potential step size produced no further change in results; a step size of 0.5 mV was generally sufficient. Convergence conditions were particularly crucial at lower pH where rates of protonation are larger. Calculation of a full set of data required approximately 60 s on a Pentium 120 MHz computer. As described elsewhere,[21] either the Butler−Volmer equation or Marcus theory (with a range of different combinations of parameters) can be used to model electron-transfer kinetics. We found that good fits could be obtained in either case and the proton-transfer parameters obtained were invariant. The results to be described in this paper were therefore obtained using the Butler−Volmer formulism, since it provided greater simplicity without compromising the fit.

Kinetic experiments in solution were performed with a PC-controlled Hi-Tech SF61 stopped-flow spectrophotometer (Hi-Tech, Salisbury, U.K.) equipped with a W light source. The cell block with mixing chamber was thermostated at 3 °C and enclosed in an anaerobic glovebox (Belle Technology, U.K.) under a nitrogen atmosphere ($O_2$ < 2 ppm). Buffers used in the kinetic studies were identical to those used in the direct electrochemical experiments but additionally contained 0.1 mM EGTA (Aldrich); the pH values of waste solutions were checked after each experiment. Samples of the one-electron reduced protein (in the $[3Fe-4S]^0$-$H^+$ state) at concentrations in the range 50−160 $\mu$M were prepared electrochemically by anaerobic bulk electrolysis and transferred immediately to the drive syringe (the cell used for bulk electrolysis has been described previously[27a]). For this preparation, tobramycin (1−2 mM, Sigma) was used to promote a diffusional electrochemical response, although we ascertained that the kinetic data were unchanged when polymyxin (the coadsorbate used in protein-film experiments) was added to the solution. Two different oxidants were used: $K_3[Fe(CN)_6]$ (BDH, AnalaR) was used without further purification, while $[Ru(NH_3)_6]Cl_3$ (Johnson Matthey) was recrystallized several times.[43] Solutions of these (in at least 10-fold excess of the protein concentration) were placed in the other drive syringe. Cluster reoxidation was monitored using the change in absorbance at 400 nm (with $[Ru(NH_3)_6]^{3+}$) or 460 nm (with $[Fe(CN)_6]^{3-}$).

## Results and Discussion

**I. Electrochemistry. A. Voltammetry of the D15N Mutant. 1. Qualitative Assessment.** In work previously reported, the D15N mutant was studied voltammetrically at scan rates of up to 1 V $s^{-1}$, and $k_{off}$ (the first-order rate constant for deprotonation) was determined as 3 $s^{-1}$.[25] In the study now described, greatly increased scan rates were used, and the model outlined in Scheme 1 was put to more stringent test. First, using pH values below the p*K* of 6.9, it was established whether excursions to high potential might reveal a second oxidation peak, the idea being that rapid imposition of a large driving force might induce *direct* oxidation of $[3Fe-4S]^0$-$H^+$. This could occur either as a concerted electron−proton transfer process (corresponding to the diagonal of Scheme 1) or a stepwise process via the species $[3Fe-4S]^+$-$H^+$ which is expected to be very acidic and have a high reduction potential, $E_{acid}$.[26] No evidence was found for either of these two pathways; cycles were recorded with oxidative switching potentials as high as 500 mV, at pH values as low as 3.8, and with scan rates up to 100 V $s^{-1}$, but only broad, irreversible features were observed which led to film degradation.

For each experiment, the electrode and protein sample were conditioned in exactly the same way before commencing the scan. Typically the potential was poised at −0.65 V for 20 s (to stabilize the film) and then at −0.15 V for 10 s (to ensure complete oxidation and deprotonation of all the clusters), following which the cycle was initiated from this potential. Representative voltammograms obtained for three pH values at slow, intermediate, and fast scan rates are shown in Figure 2. Qualitative inspection shows that the voltammetry follows the predictions of Scheme 1, according to which we expect three types of behavior depending on both the pH (more exactly, pH − p*K*) and the scan rate.

**a. "Thermodynamic" Electron and Proton Transfer.** At slow scan rates (e.g., 10 mV $s^{-1}$), equilibration occurs to give thermodynamically determined populations of all contributing species (i.e., $[3Fe-4S]^+$, $[3Fe-4S]^0$, and $[3Fe-4S]^0$-$H^+$) according to pH and potential. The reductive and oxidative waves are symmetrical and Nernstian, the half-height widths are close to the ideal one-electron value, and the peak separation is close to zero.[20,21] The shift in reduction potential as the pH is lowered is in accordance with equation 1, in which $E_{alk}$ is the limiting

$$E_{(pH)} = E_{alk} + \frac{RT}{F}\ln\left\{1 + \frac{[H^+]}{K_{red}}\right\}$$

$$[H^+] = 10^{-pH} \qquad K_{red} = 10^{-pK_{red}} \tag{1}$$

value of the reduction potential at high pH where no proton is transferred. The resulting p*K* for $[3Fe-4S]^0$ is 6.9.[26]

**b. Gating.** At 1 V $s^{-1}$, the voltammetry becomes increasingly asymmetric as the pH is lowered; the reduction waves

(38) Bard, A. J.; Faulkner, L. R. *Electrochemical Methods*: *Fundamentals and Applications*; Wiley: New York, 1980.

(39) Armstrong, F. A. In *Bioelectrochemistry of Biomacromolecules*: *Bioelectrochemistry*: *Principles and Practice*; Lenaz, G., Milazzo, G., Eds.; Birkhauser Verlag: Basel, 1997; pp 205−255. Armstrong, F. A.; Butt, J. N.; Sucheta, A. *Methods Enzymol.* **1993**, *227*, 479−500. Armstrong, F. A. *Adv. Inorg. Chem.* **1992**, *38*, 117−163.

(40) Britz, D. *J. Electroanal. Chem.* **1978**, *88*, 309−352.

(41) Press, W. H.; Flannery, B. P.; Teukolsky, S. A.; Vetterling, W. T. *Numerical Recipes in Pascal*; Cambridge University Press: New York, 1989.

(42) Britz, D. *Digital Simulation in Electrochemistry*, 2nd ed.; Springer-Verlag: Berlin, 1988.

(43) Pladziewicz, J. R.; Meyer, T. J.; Broomhead, J. A.; Taube, H. *Inorg. Chem.* **1973**, *12*, 639−643.

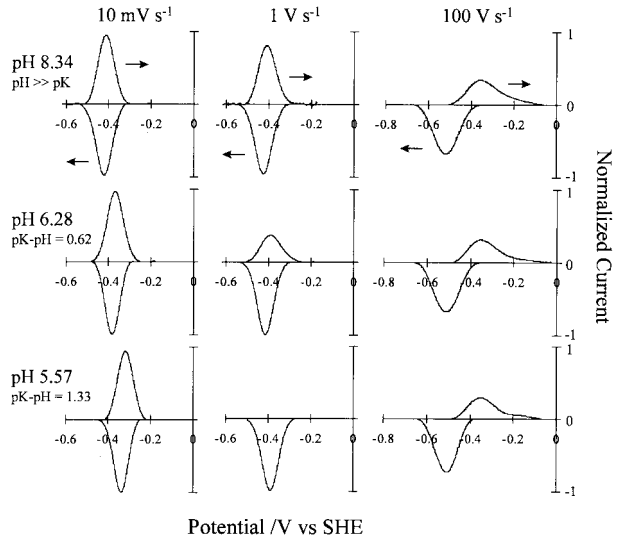


**Figure 2.** Background-corrected voltammograms recorded for D15N. In each case the peaks have been normalized to a Nernstian peak height of unity (*y*-axis). Arrows indicate directions of scanning. Conditions: temperature 0 °C, 20 mM mixed buffer, polymyxin 200 $\mu$g ml$^{-1}$, 0.1 M NaCl, potential poised for 20 s at −0.650 V and then for 10 s at −0.150 V. From left to right the scan rates are 10 mV s$^{-1}$, 1 V s$^{-1}$, and 100 V s$^{-1}$ and from top to bottom, pH 8.34, 6.28 (pH − p$K$ = 0.62), and 5.57 (pH − p$K$ = 1.33), showing clearly the time domains for thermodynamic control, gating, and electron-transfer-only behavior.

remain sharp whereas the oxidation waves become broadened and severely attenuated, eventually vanishing into the background. As discussed later, the behavior is not that expected of a *concerted* electron−proton transfer (which in the simplest case would reversibly follow a reaction coordinate crossing Scheme 1 diagonally and produce a symmetrical voltammogram regardless of scan rate). In contrast, the results show that the oxidation reaction becomes "gated" by a preceding process, that is, oxidation of $[3Fe-4S]^0$-$H^+$ cannot occur unless the cluster first releases the proton. In electrochemical terminology, the reduction reaction is "EC" and the reoxidation is "CE".[36,38] The reductive process requires no preceding chemical conversion and is thus never gated. At the top of Figure 2 is the behavior recorded for pH 8.34; since the p$K_{red}$ is 6.9, protonation of the reduced cluster does not occur and so the scans remain uncomplicated. At pH 6.28, however, it is apparent that the oxidative process is retarded, and at pH 5.57 (bottom of Figure 2) the oxidative peak is absent, indicating the cluster is effectively locked in the protonated and reduced state.

**c. Electron Transfer Only: "Uncoupling".** The right-hand panel of Figure 2 shows voltammograms measured at 100 V s$^{-1}$. The signals each have the same reduction potential and peak shapes, even though the pH values differ, because the protonation of $[3Fe-4S]^0$ is now being outrun, that is, reoxidation is initiated before the proton can transfer to the cluster. Apart from some asymmetry, evident as a tail in the oxidative peak, the behavior in each case is that of a simple, fast electron-transfer couple.

**2. Quantitative Assessment.** The aim is now to determine the form of the rate law involving $k_{on}$ and $k_{off}$ (Scheme 1). First, the electron-transfer-only behavior was modeled using the Butler−Volmer equation (eq 2). Here, $k_{red}$ and $k_{ox}$ are potential-dependent rate constants for reduction and oxidation, respectively, $k_0$ is the standard (exchange) rate constant at zero overpotential (note that these are *first-order* rate constants for the surface-confined system), and $\alpha$ is the transfer coefficient, which we fixed at 0.5.[21,38] The model predicts that the peaks separate symmetrically from the reduction potential ($E°'$) as the scan rate is increased.

$$k_{red} = k_0 \exp\{-\alpha nF(E - E°')\} \text{ and}$$
$$k_{ox} = k_0 \exp\{(1 - \alpha)nF(E - E°')\} \quad (2)$$

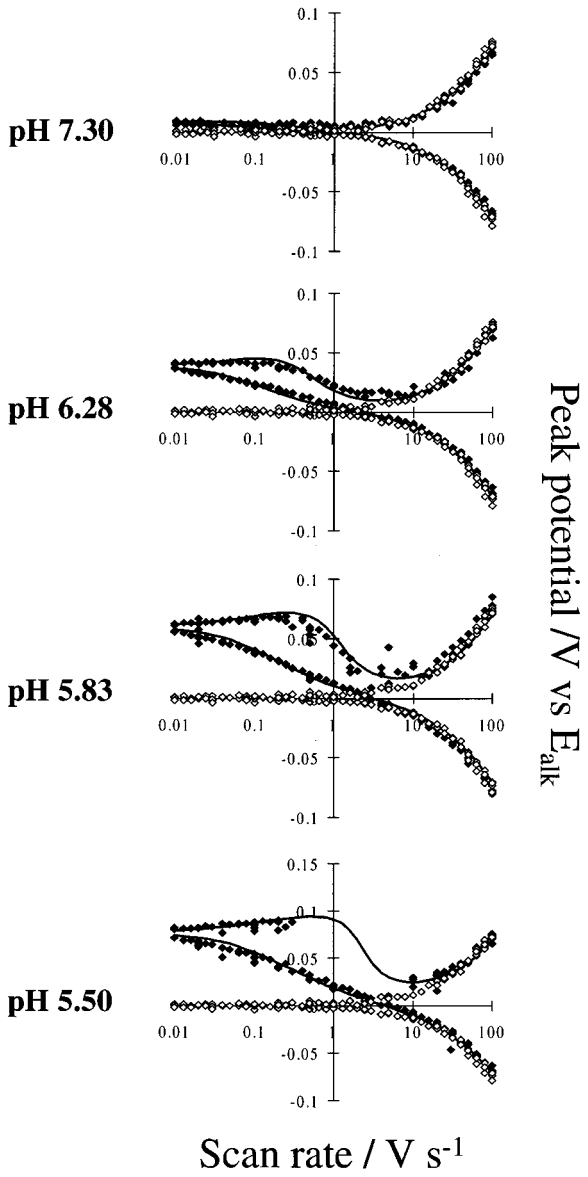


**Figure 3.** Peak positions (vs $E_{alk}$) for D15N as a function of scan rate (log scale) for a range of different pH values (solid symbols). Also shown (open symbols) are the peak positions recorded at the alkaline limit (pH 8.34) and the lines predicted by the model.

As discussed elsewhere,[21] there are some minor irregularities in the electron-transfer kinetics of D15N, especially when the potential is poised at the oxidative limit before commencing the scan. We note, however, that the peak separations are little affected by the poising potential, although the average peak potential $E°$ shifts slightly (ca. −20 mV) with scan rate. To simplify our analysis, we corrected all data for this small shift in $E°$ and for the constant peak separation at low scan rate, using factors obtained from experiments at pH 8.34. Reduction potentials at lower pH also needed to be adjusted for the effects attributable to protonating remote residues in the protein matrix, amounting to a maximum correction of 12 mV at pH 5.50. Figure 3 shows data recorded at pH values of 7.30, 6.28, 5.83, and 5.50, where in each case the fast "electron-transfer-only"

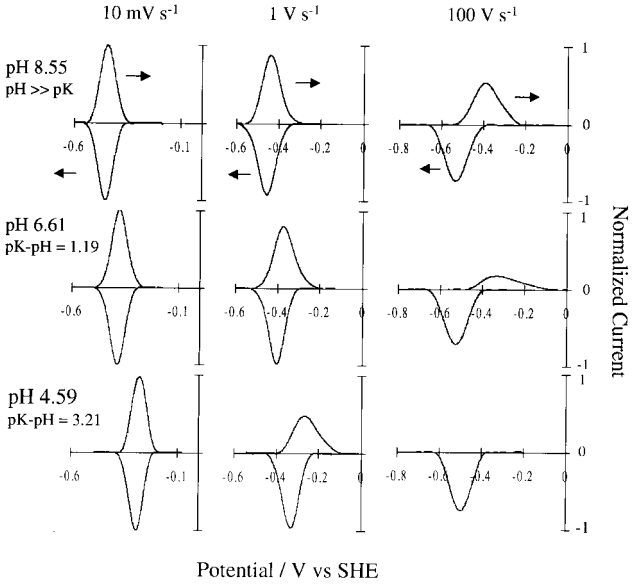


**Figure 4.** Background-corrected and normalized voltammograms recorded for native Fd I. Arrows indicate directions of scanning. Conditions: temperature 0 °C, 20 mM mixed buffer, polymyxin 200 $\mu$g ml$^{-1}$, 0.1 M NaCl, potential poised for 20 s at −0.650 V and then for 10 s at −0.150 V. From left to right, the scan rates are 10 mV s$^{-1}$, 1 V s$^{-1}$, and 100 V s$^{-1}$ and from top to bottom, pH 8.55, 6.61 (pH − p$K$ = 1.19), and 4.59 (pH − p$K$ = 3.21), showing clearly that proton transfer in native Fd I is significantly faster than in D15N.

behavior recorded at pH 8.34 is included for comparison. At a low scan rate, the behavior is always reversible and thermodynamic; as the scan rate is increased the oxidation becomes gated, and at lower pH (5.50) the peak disappears between 0.5 and 10 V s$^{-1}$. At still higher scan rates, both oxidative and reductive peak positions become superimposable on the pH 8.34 "electron-transfer-only" data.

Also shown in Figure 3 are the predictions of Scheme 1 simulated using the finite difference procedure. An almost perfect fit is obtained over the *entire* pH range with a single set of parameters: $E_{alk} = -0.408$ V, $k_0 = 550$ s$^{-1}$, p$K = 6.9$, and a deprotonation rate $k_{off} = 2.52$ s$^{-1}$ that is independent of potential. Rates of cluster protonation and deprotonation are therefore given by eqs 3A and 3B.

$$\text{rate}_{on} = k_{on}\,[H^+]\{[3Fe{-}4S]^0\}_{surf} \qquad (3A)$$

$$\text{rate}_{off} = k_{off}\,\{[3Fe{-}4S]^0\text{-}H^+\}_{surf} \qquad (3B)$$

Limited experiments were also carried out in $D_2O$ at two p$D$ values, one at the "electron-transfer-only" limit and one at lower p$D$: in order to obtain a good fit, $k_{off}$ was required to decrease from 2.5 to 1.5 s$^{-1}$.

**B. Voltammetry of Native *Av* Fd I.** Previous work on the native *Av* Fd I protein, at scan rates up to 1 V s$^{-1}$, indicated that rates of cluster protonation and deprotonation were much faster than for D15N. Indeed, no kinetic complications could be identified over this timescale.[25] The faster scan rates now applied, however, have allowed us to study the kinetics of coupled proton transfer in this much more active system. Figure 4 shows a set of voltammograms for native *Av* Fd I for comparison with those shown in Figure 2 for D15N. The reduction potential at the alkaline limit (−0.443 V) is more negative than that for D15N, and the p$K_{red}$ of the cluster is 7.8 instead of 6.9, mainly because of the presence of the negatively charged carboxylate instead of the neutral carbamide.[26] As before,

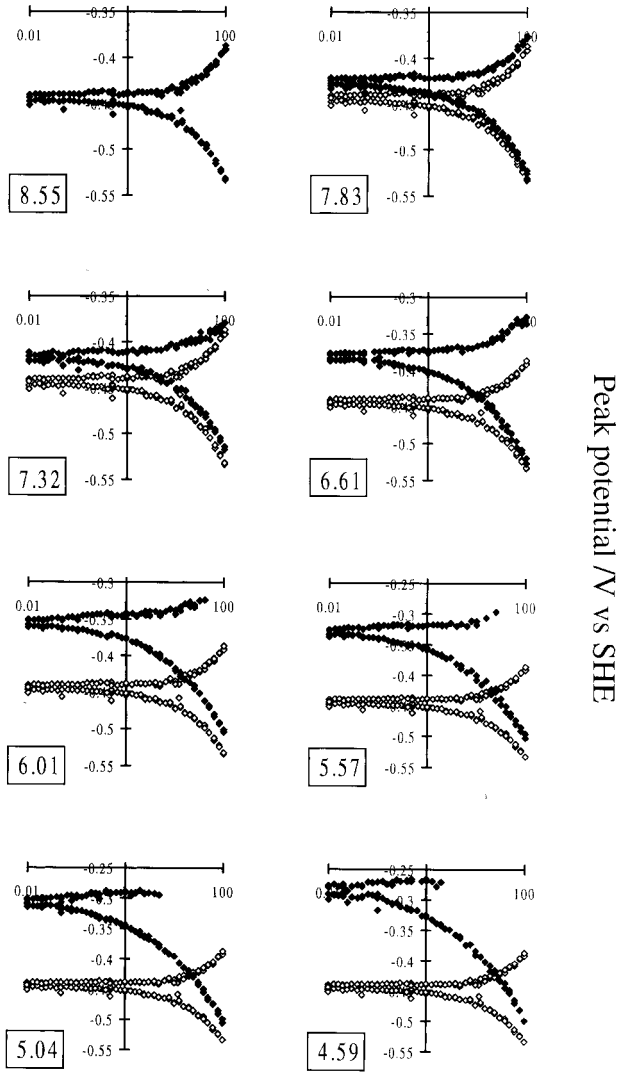


**Figure 5.** Peak positions (vs SHE) for native Fd I (closed symbols) as a function of scan rate (log scale) for a range of different pHs (boxed). Also shown (open symbols) are the peak positions recorded at pH 8.55, effectively at the alkaline limit.

excursions to high potential revealed no additional features, and as discussed below, analysis was pursued in terms of the stepwise model proposed for D15N. The results reveal much faster proton-transfer rates; only at the lowest pH and the highest scan rate does the oxidative peak disappear, and the electron-transfer limiting behavior so readily observable for D15N is never obtained at any pH lower than the alkaline limit. Figure 5 shows the variation of peak potential with scan rate for a range of pH values; in each case the results are displayed alongside data obtained at pH 8.55, that is, where $E^{\circ\prime}$ is close to $E_{alk}$.

Data for native *Av* Fd I were also analyzed using the finite difference procedure.[21,42] First, the electron transfer at high pH (8.55) was modeled, utilizing small corrections to the dataset in order to produce a good fit as described elsewhere.[21] Data for all the other pH values were corrected in an identical fashion. The fit obtained for pH 8.55 is included in Figure 6. Stepwise protonation and deprotonation steps were then included as above, but it was immediately clear that the simple bimolecular proton-transfer mechanism observed for D15N does not apply; in particular it was evident that cluster oxidation slows down as the pH is decreased. Two changes to the model were required

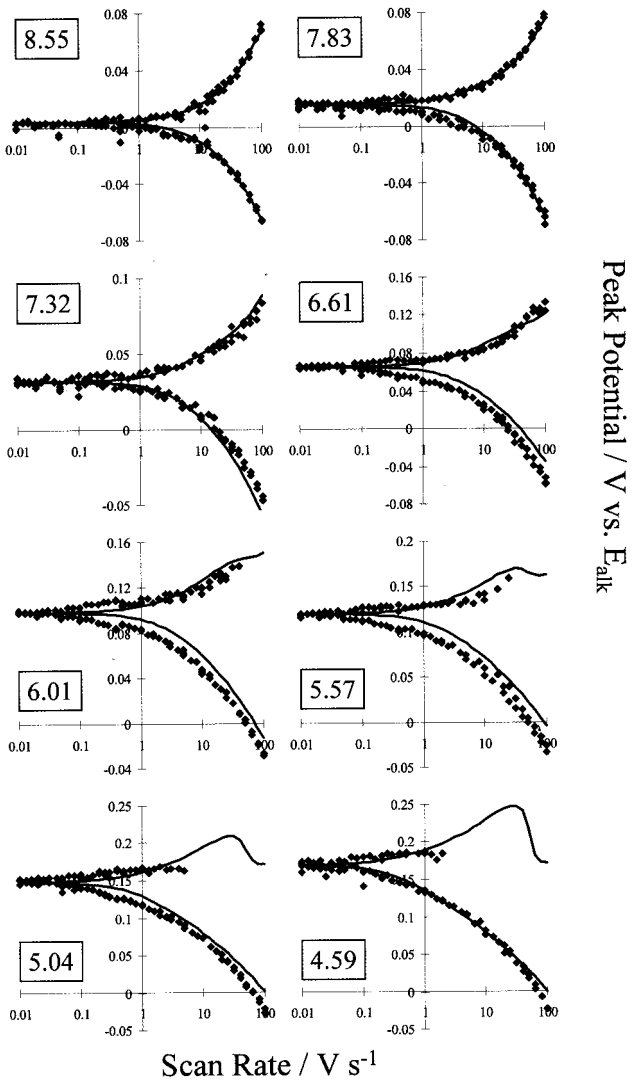


**Figure 6.** Modeling of the corrected data for native Fd I using the parameters in Table 1 (pH values boxed). In each case, the experimentally determined peak positions are shown as solid symbols and the fit obtained is shown as a line.

**Scheme 2.** Kinetic Mechanism of Protonation of $[3Fe-4S]^0$ in Native *Av* Fd I

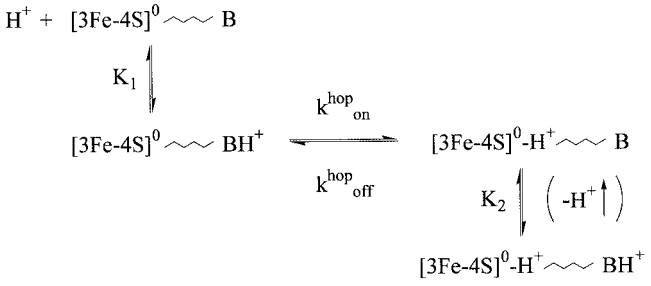


in order to obtain a satisfactory fit. First, the p$K$ of the $[3Fe-4S]^0$ cluster decreases from 7.8 at high pH to 6.5 at low pH; second, the first-order rate constant for deprotonation, $k_{off}$, decreases as the pH is lowered, from a maximum value at high pH. The optimal fit thus obtained gave the lines shown in Figure 6, alongside the corrected data, at each pH value. Although there remain differences between the optimized fit and the data, particularly in the intermediate pH region, it should be borne in mind that these usually amount to less than 10 mV, and attempts to alter the parameters always resulted in greater deviation. To avoid overcomplicating the analysis, no further refinements were made.

These results can be rationalized in terms of a "hopping" mechanism, depicted in Scheme 2, in which the proton shuttles between a surface base (B) and the buried cluster; the zigzag line represents a barrier to proton transfer. The profound difference between native Fd I and the D15N mutant, as determined from both the voltammetry and the homogeneous kinetics (see below), identifies this base as the D15 carboxylate. To simplify the analysis, proton exchanges between the base and solvent are assumed to be in rapid equilibria, with $K_1$ and $K_2$ defined as dissociation constants.

The first stage in cluster protonation is the binding of a proton to B ($1/K_1$). The proton then transfers to the cluster ($k^{hop}_{on}$) and another proton may then bind to B ($1/K_2$). The reverse reaction requires that the base is vacant to accept the proton from the cluster, thus any $BH^+$ must first become deprotonated ($K_2$). The optimized parameters, derived from numerical simulation and according to Scheme 2, are given in Table 1 along with directly comparable data for D15N. The electron-transfer rate constants ($k_0$) required to optimize the fit across the whole range are high and close to those determined at pH 8.34.[21] For clarity, the terms p$K_1$ and p$K_2$ refer to D15, whereas p$K_{cluster}$ refers to $[3Fe-4S]^0$ (i.e., p$K_{red}$ as defined above).

The rate laws can be written as eqs 4A and 4B. Due to the

$$\text{rate of protonation} = k^{hop}_{on}\frac{[[3Fe-4S]^0][H^+]}{[H^+]+K_1} \quad (4A)$$

$$\text{rate of deprotonation} = k^{hop}_{off}\frac{[[3Fe-4S]^0][H^+]K_2}{[H^+]+K_2} \quad (4B)$$

close proximity of the D15 carboxylate and the cluster, there is electrostatic interaction between the two sites of protonation, thus p$K_2$ < p$K_1$, and p$K_{cluster}$ decreases from 7.8 to 6.5 when the carboxylate is protonated. Obviously there is also a corresponding and opposite effect on $E_{alk}$, such that the equilibrium reduction potential observed at a given pH remains unchanged. The situation is similar to that found for D15N, where replacement of the carboxylate by neutral carbamide causes the p$K_{red}$ of the cluster to decrease to 6.9 and $E_{alk}$ to increase.[26] Note also that since p$K_1$ > p$K_2$, the D15 carboxylate becomes a weaker base when $[3Fe-4S]^0$ is protonated. The relationships between the p$K$ values for cluster and carboxylate are shown in Scheme 3, where closed squares indicate that a proton is bound.

**Scheme 3.** Relationships between the p$K$ Values of Cluster and Base upon Sequential Protonations

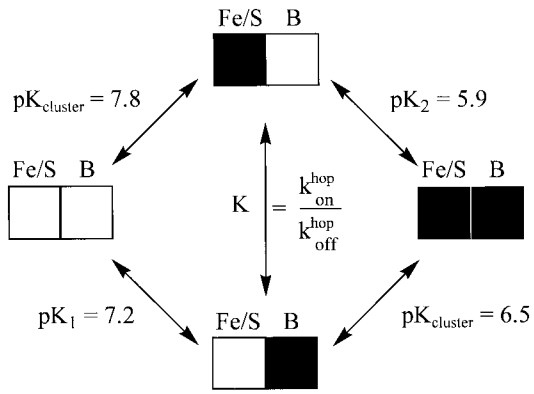

**Table 1.** A Compilation of Results Obtained for D15N and Native Forms of *Av* Fd I

| | $E_{alk}$ (V) | $k_0$ ($s^{-1}$) | p$K_{cluster}$ high pH | p$K_{cluster}$ low pH | p$K_1$ (D15) | p$K_2$ (D15) | $k^{hop}_{on}$ ($s^{-1}$) | $k^{hop}_{off}$ ($s^{-1}$) |
|---|---|---|---|---|---|---|---|---|
| D15N | −0.408 | 550 ± 25 | 6.9 ± 0.05 | 6.9 ± 0.05 | | | | |
| Av Fd I | −0.443 | 600 ± 25 | 7.8 ± 0.05 | 6.5 ± 0.1 | 7.2 ± 0.1 | 5.9 ± 0.1 | 1294 ± 100 | 332 ± 25 |

The equilibrium constant for proton transfer between the base and the cluster, given by $k^{hop}_{on}/k^{hop}_{off}$ is determined thermodynamically to be $10^{0.6}$ or ∼ 4, in agreement with the values given in Table 1.

As a qualitative test of the model, an additional experiment was carried out to confirm the ability of the system to recover activity after a reductive poise, under conditions where all reduced clusters are loaded with a proton (pH ≪ p$K_{cluster}$). In each case, the potential was held at the reductive limit and then cycled around to reach different oxidizing potentials. Obviously, the time allowed for deprotonation to occur depends on the time needed to reach the oxidative limit and return to $E_{(pH)}$; as predicted, the subsequent reduction peak increased in magnitude as this limit was raised. Results for both D15N and native Fd at pH 5.17 are shown in Figure 7. It was a simple matter to "tune" the scan rate to the value required to differentiate between fully trapped and fully "escaped" clusters at the two extremes; accordingly, scan rates of 1 and 20 V $s^{-1}$, respectively, were required for D15N and *Av* Fd I, consistent with the ratio of $k_{off}$ values at pH 5.17 ( 2.5/50.5 or ∼1/20), the pH-dependent value for native Fd I being calculated from the model.

**II. Stopped-Flow Kinetics.** Stopped-flow spectrophotometry provided an independent method of measuring the rate of oxidation of the cluster and therefore, under conditions of gating, the rate of deprotonation, $k_{off}$ in Scheme 1. The kinetics of interest are described by the reaction sequence shown in Scheme 4.

**Scheme 4.** Reaction Sequence for Studying Cluster Deprotonation by Stopped-Flow Spectrophotometry

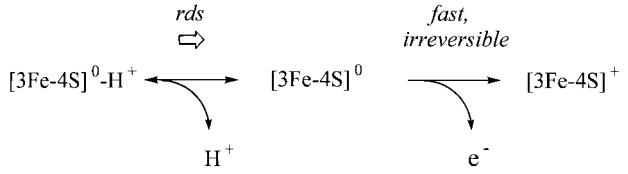


Provided that oxidation of $[3Fe-4S]^0$ is rapid and irreversible, the rate of formation of $[3Fe-4S]^+$ from $[3Fe-4S]^0$-$H^+$ is limited by the rate of deprotonation, which should be independent of the driving force (concentration and reduction potential of oxidant).[44]

Reactions were carried out with either $[Fe(CN)_6]^{3-}$ ($E^{\circ\prime}$ = 358 mV) or $[Ru(NH_3)_6]^{3+}$ ($E^{\circ\prime}$ = 100 mV) as oxidants. Each of these are outer-sphere reactants with high intrinsic activities.[45] Some representative results are shown in Figure 8. (A) At pH 8.5, oxidation of $[3Fe-4S]^0$ for each protein is complete within the instrument deadtime for either oxidant at all concentrations. This was as expected since both oxidants have high self-exchange rate constants and the driving force is very favorable. (B) At pH 6.7, oxidation of native Fd I displays first-order kinetics, with an average rate constant of 276 ± 89 $s^{-1}$ that is independent of the nature or concentration of oxidant. For these experiments, higher concentrations of protein were used to improve the signal-to-noise ratio. (C) Much slower kinetics

(44) Wilkins, R. G. In *Kinetics and Mechanism of Reactions of Transition Metal Complexes*; VCH: Weinheim, 1991; pp 15 and 16.

(45) Lappin, A. G. *Redox Mechanisms in Inorganic Chemistry*; Ellis Horwood: Chichester, 1994.

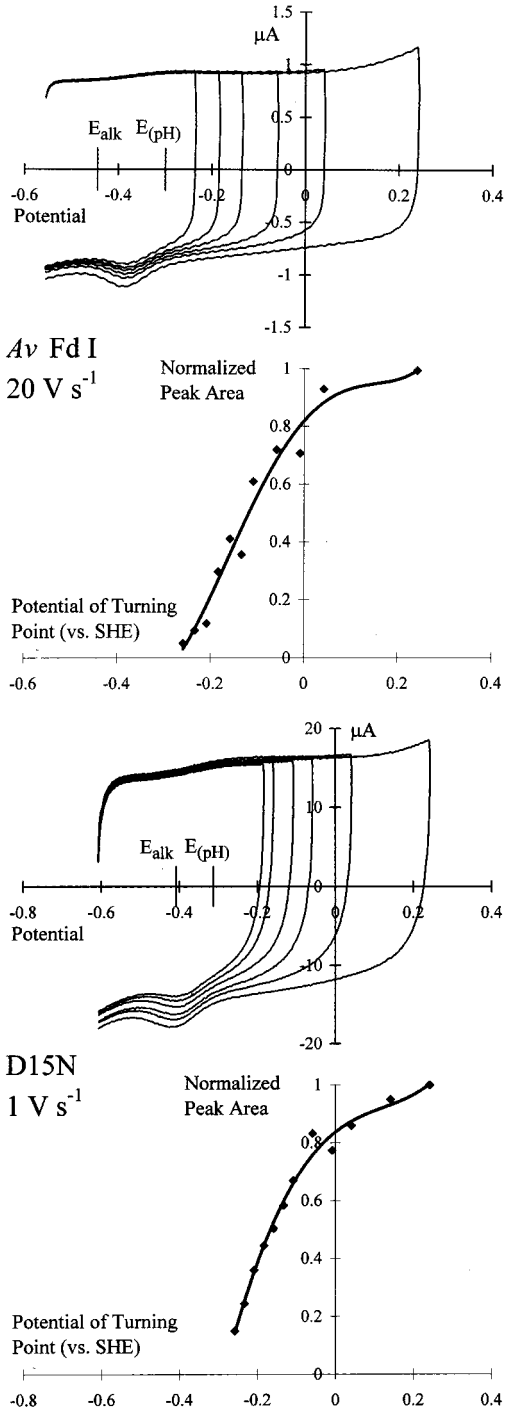


**Figure 7.** Voltammograms showing how scanning to different oxidizing potentials allows different degrees of escape of $[3Fe-4S]^0$ clusters from the protonated state. In each case the potential was prepoised at the reductive limit before scanning. Voltammetry of D15N was carried out at 1 V $s^{-1}$ and pH 5.17, while voltammetry of native Fd I was carried out at 20 V $s^{-1}$ and pH 5.17, the chosen conditions being consistent with the ratios of $k_{off}$ at this pH. Also shown are the variations in normalized areas of the following reduction peaks with oxidative switching potential, the position of $E_{alk}$, and the position of the pH-dependent reduction potential $E_{(pH)}$.

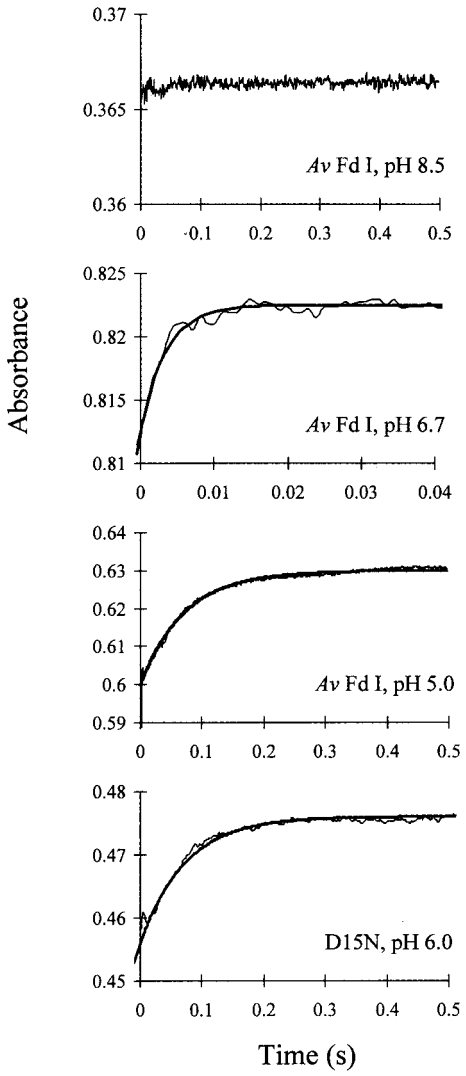


**Figure 8.** Stopped-flow traces showing oxidation of the $[3Fe-4S]^0$ cluster in native Fd I and D15N by $[Ru(NH_3)_6]^{3+}$ or $[Fe(CN)_6]^{3-}$ at different pH values. Conditions in each case: temperature 3 °C, 20 mM mixed buffer, and 0.1 M NaCl. From top to bottom: (A) native Fd I (25 $\mu$M) at pH 8.5, oxidant 0.25 mM $[Ru(NH_3)_6]^{3+}$, the reaction is ungated and complete in the instrument dead time (similar result obtained using $[Fe(CN)_6]^{3-}$); (B) native Fd I (80 $\mu$M) at pH 6.7, oxidant is 1.6 mM $[Fe(CN)_6]^{3-}$, rate constant is 290 $s^{-1}$; (C) native Fd I (40 $\mu$M) at pH 5.0, oxidant is 1.0 mM $[Fe(CN)_6]^{3-}$, rate constant is 27.9 $s^{-1}$; (D) D15N (25 $\mu$M) at pH 6.0, oxidant is 0.25 mM $[Fe(CN)_6]^{3-}$, rate constant is 13.1 $s^{-1}$.

are observed at pH 5.0, at which value oxidation of native Fd I occurs with an average rate constant of $25.9 \pm 2.7$ $s^{-1}$. In all cases, the kinetics are independent of the nature or concentration of oxidant. (D) At pH 6.0, oxidation of D15N occurs with an average rate constant of $14.1 \pm 1.0$ $s^{-1}$. Experiments at pH 5.0 gave $12.7 \pm 0.7$ $s^{-1}$, all independent of the nature or concentration of oxidant.

Two sets of experiments were carried out to ascertain whether the oxidation reaction shows a deuterium isotope effect. First, native Fd I was studied at pD 6.7. Rate constants measured with either $[Ru(NH_3)_6]^{3+}$ or $[Fe(CN)_6]^{3-}$ showed no significant variation (within error), and the average value was 223 $s^{-1}$. Likewise, the oxidation of D15N was studied at pD 6.0, using both $[Ru(NH_3)_6]^{3+}$ and $[Fe(CN)_6]^{3-}$ as oxidants. No significant difference was observed between the two reactants, and an average rate constant of $6.3 \pm 0.2$ $s^{-1}$ was obtained. Individual rate constants are included in Table 2, which also compares values of $k_{off}$ measured by stopped-flow spectrophotometry and voltammetry.

**Table 2.** A Comparision of Rate Constants for Deprotonation of $[3Fe-4S]^0$-$H^+$ As Measured by Stopped-Flow Spectrophotometry or Voltammetry

| protein | pH | $k_{off}$ (stopped-flow) ($s^{-1}$) | $k_{off}$ (voltammetry) ($s^{-1}$) |
|---|---|---|---|
| D15N | 8.0 | not meas[a] | $2.5 + 0.1$ |
| D15N | 6.0 | $14.1 \pm 1.0$ | $2.5 + 0.1$ |
| D15N | 5.0 | $12.7 \pm 0.7$ | $2.5 + 0.1$ |
| D15N, $D_2O$ | 6.0 | $6.3 \pm 0.2$ | $1.3 + 0.1$ |
| native *Av* Fd I | 8.0 | not meas[a] | $319 + 25$ |
| native *Av* Fd I | 6.7 | $276 \pm 89$ | $278 + 25$ |
| native *Av* Fd I | 5.0 | $25.9 \pm 2.7$ | $36 + 5$ |
| native *Av* Fd I, $D_2O$ | 7.2 | $223 \pm 41$ | |
| native *Av* Fd I, $D_2O$ | 6.7 | $223 \pm 41$ | |

[a] ET controlled; the rate constant is for deprotonation occurring in such a small population of $[3Fe-4S]^0$-$H^+$ that the reaction would be ineffective as a gate and would not be detected by stopped-flow.

## General Conclusions

The results show how, with a single set of experiments, it is possible to recognize coupled reactions and to deconvolute the results in a quantitative manner. Dealing first with the overall pattern of the electron−proton coupling, the results show that in a cycle starting from the oxidized form, the reactions occur in a stepwise not a concerted manner, that is, electron−proton/proton−electron (ECCE in electrochemical terms[36]). First, a near-perfect fit is obtained for D15N, the model requiring protonation of the reduced cluster with simple bimolecular proton-transfer kinetics, followed by reoxidation which is gated by a chemical reaction having a rate constant that is not only independent of pH but also of electrode potential. The ability to outrun cluster protonation and thus decouple the electron and proton transfers by cycling back rapidly eliminates a concerted mechanism for the reduction direction. For oxidation, the lack of a driving force dependence, either observed or modeled in the voltammetry or as measured in the stopped-flow experiments, again argues against a concerted mechanism in which simultaneous transfer of the proton would be embodied into and contribute to the electron-transfer reorganization energy.[5,37] These arguments apply also to native Fd I. Although, on starting from the oxidized form, it is not possible to decouple the subsequent protonation process completely, increases in scan rate do cause a marked shift in the reduction potentials toward the uncoupled electron-transfer-only values ($E_{alk}$). For both native *Av* Fd I and D15N, raising the scan rate causes the oxidation wave to broaden and flatten out as expected for rate-limiting (potential-independent) proton transfer.

Next, dealing with the stepwise events, the excellent fit obtained for D15N confirms slow but simple bimolecular proton-transfer kinetics, while that obtained for native *Av* Fd I requires an intramolecular proton-hopping mechanism. In the latter case, considering the wide range of pH over which the data have been fitted, the overall agreement is very good, and although further improvements might be achieved by including additional coupling (i.e., extending Scheme 1), the appealing simplicity of the model would be sacrificed. For both variants, electron transfer is intrinsically fast in either direction, but once a proton has entered the cluster, reoxidation is gated by the rate of its release. Such kinetics are typically measured by conventional methods, in which case forward and reverse directions are viewed in separate, often unconnected experiments. Here we have been able to measure the rate constants

for reoxidation independently using stopped-flow spectrophotometry. For native *Av* Fd I, excellent agreement is obtained between results provided by electrochemistry and stopped-flow, thus not only providing support for the overall integrated picture derived by voltammetry but also showing that protein activity is not affected by the binding to the electrode surface. On the other hand, for D15N deprotonation is retarded when the protein is adsorbed on the surface, suggesting that motions required to allow this much slower proton transfer to occur have become restricted. The relative magnitudes of the isotope effects, approximately 2 for D15N and only slight, if any, for *Av* Fd I, indicate that proton tunneling is not a limiting factor, especially in the native protein.[6]

Scheme 3 shows four states of the native Fd I $[3Fe-4S]^0$ system, three of which are thermodynamically stable, with the fourth state (bottom; Fe/S deprotonated, B protonated) being unstable and invoked as a transient intermediate. The p*K* of the cluster in this state is decreased from 7.8 to 6.5, so that it is even less basic than the cluster in D15N (6.9). The p*K* of the base shifts from 7.2 to 5.9 as the proton moves onto the $[3Fe-4S]^0$ cluster. It is reasonable to expect (as supported by the structural data[34]) that the electrostatic influence of the reduced protonated cluster resembles most that of the oxidized cluster for which NMR indicates that the p*K* of the D15 carboxylate is 5.4.[35]

The dramatic effect of changing aspartate to asparagine and the fit of data to the order of events shown in Scheme 2 together provide firm evidence for the role of the D15 carboxylate in relaying protons. We also observe how interaction between the [3Fe−4S] cluster and the carboxylate influences this process. Arrival of the electron on the cluster raises the carboxylate p*K* from ca. 5.4 (NMR, measured for the oxidized form) to 7.2 (modeled), and the greatly increased ability of D15 to capture a proton from solvent thereby facilitates cluster protonation. The proton thus travels into the protein "in the slipstream of the electron". This sequence of events resembles part of the cycle of a redox-driven proton pump. An obvious shortcoming is that oxidation of the protonated reduced cluster $[3Fe-4S]^0$-$H^+$, to complete the cycle of Scheme 1 and then release $H^+$ spontaneously (an ECEC sequence[36]), requires a potential that is too high for practical purposes; instead the proton must first be released by reversal of the sequence.[46] Electron transfer in the oxidation direction is thus gated. However, proton transfer can be decoupled by speeding up the scan rate, and we observe that the reduction potential drops to that observed under alkaline conditions. This is an example of measurement of the reduction potential of a couple involving a transient state.[47]

The "hopping" model can account for the large attenuation of rates in D15N because the carbamide group is such a weak base that it is able neither to capture the incoming proton from solvent nor to receive the escaping proton from the cluster (see Scheme 2). However, even with the native protein, there is still the question of how the proton is transferred into the protein. The lack of a significant isotope effect and the absence of other intervening sites in the structure, including $H_2O$ molecules, suggest strongly that the proton is shuttled between the carboxylate and the cluster by a "piggy back" mechanism involving relative movement of the carboxylate side chain.[9,11] The time constants for this process, of the order of a millisecond, are indeed typical of those reported for rate-determining events in proton-translocating enzymes.[4]

The following hypothesis is presented on the basis of the crystallographic evidence available to date.[34] Consider proton transfer from the cluster back to D15, which can be discussed in terms of the structure of the $[3Fe-4S]^0$ protein studied at pH 6. As depicted in Figure 1, the closest distance between a protonatable carboxylate oxygen atom of D15 (O2) and a cluster atom (S1) is 4.85 Å. We need to assume that wherever the proton is bound on the cluster, it can be moved easily to the S1 position. An estimate for the minimum gap in the proton pathway from cluster S1 to O2 is then 4.85 (S1−O2 distance) − 1.3 (S−H bond) − 1.2 (covalent radius of hydrogen atom) − 1.5 (van der Waals radius of oxygen atom) = 0.85 Å.[48] However, if we invoke some mobility of the D15 side chain, all that is required is a small rotation about the $-CH_2-$ linker and, in the extreme case, a 180° rotation would decrease the S1−O2 distance to 2.04 Å. The same calculations show that this is more than enough to achieve proton transfer at van der Waals contact, and indeed a much smaller movement would suffice. Proton exchange between the O2 atom and solvent $H_2O$ molecules completes the process. That the D15 side chain may indeed be reasonably mobile with respect to the cluster may be expected from the observation that the O2−S1 distance is increased at pH 8, corresponding to the $[3Fe-4S]^0$ cluster being unprotonated.[34,49]

The *Av* Fd I system thereby provides a new model for the study of redox coupling and proton transfer in proteins, an important feature being that it becomes possible to relate the observations to usefully localized features of protein structure. Notably, the coupling and side-chain motions that provide the proton courier in Fd I are relevant in mechanisms that have been proposed for enzymes such as cytochrome oxidase.[13,14] Unlike these more complex systems, Fd I has been structurally characterized in many of the relevant redox/protonation states and is fully amenable to fast-scan protein-film voltammetric studies. Detailed investigations, employing further site-directed mutagenesis, molecular dynamics calculations, and structure determinations at higher resolution, are currently in progress.

**Acknowledgment.** This research was supported by grants from the UK EPSRC (GR/J84809) and The Wellcome Trust (042109) to F.A.A. and from NIH (GM-45209) to B.K.B. We are grateful to Dr. H. A. Heering and Professor C. D. Stout for helpful comments.

JA980380C

(46) An example of a complete ECEC cycle as analyzed by protein-film voltammetry is given in a study of the redox-dependent binding of a thiolate ligand to a [4Fe−4S] cluster. See: Butt, J. N.; Sucheta, A.; Armstrong, F. A.; Breton, J.; Thomson, A. J.; Hatchikian, E. C. *J. Am. Chem. Soc.* **1993**, *115*, 1413−1421.

(47) Armstrong, F. A. *J. Biol. Inorg. Chem.* **1997**, *2*, 139−142.

(48) Huheey, J. E.; Keiter, E. A.; Keiter, R. L. *Inorganic Chemistry: Principles of Structure and Reactivity*, 4th ed.; Harper Collins: New York, 1993.

(49) We have assumed that the salt bridge between D15 and K84 is weak and does not restrict the function of D15. Our results support this proposal since, if the integrity of the salt bridge was a key factor in mediating proton transfer, rates of both protonation and deprotonation would fall off at low pH; instead, only deprotonation slows down, while the rate of protonation approaches a maximum value.